On the time evolution of climate sensitivity and future warming

Philip Goodwin[1]

[1] *Ocean and Earth Sciences, University of Southampton, Southampton, UK*

P. Goodwin, ORCID ID: https://orcid.org/0000-0002-2575-8948

For submission to *Earth's Future*

16th July 2018

Abstract

The Earth's climate sensitivity to radiative forcing remains a key source of uncertainty in future warming projections. There is a growing realisation in recent literature that research must go beyond an equilibrium and CO_2-only viewpoint, towards considering how climate sensitivity will evolve over time in response to anthropogenic and natural radiative forcing from multiple sources. Here, the transient behaviour of climate sensitivity is explored using a modified energy balance model, in which multiple climate feedbacks evolve independently over time to multiple sources of radiative forcing, combined with constraints from observations and from the Climate Model Intercomparison Project phase 5 (CMIP5). First, a large initial ensemble of 10^7 simulations is generated, with a distribution of climate feedback strengths from sub-annual to 10^2 year timescales constrained by the CMIP5 ensemble; including the Planck feedback, the combined water-vapour lapse-rate feedback, snow and sea-ice albedo feedback, fast cloud feedbacks, and the cloud response to SST-adjustment feedback. These 10^7 simulations are then tested against observational metrics representing decadal trends in warming, heat and carbon uptake, leaving only 4.6×10^3 history-matched simulations consistent with both the CMIP5 ensemble and historical observations. The results reveal an annual-timescale climate sensitivity of 2.1 °C (ranging from 1.6 to 2.8 °C at 95% uncertainty), rising to 2.9 °C (from 1.9 to 4.6 °C) on century timescales. These findings provide a link between lower estimates of climate sensitivity, based on the current transient

This article has been accepted for publication and undergone full peer review but has not been through the copyediting, typesetting, pagination and proofreading process which may lead to differences between this version and the Version of Record. Please cite this article as doi: 10.1029/2018EF000889

state of the climate system, and higher estimates based on long-term behaviour of complex models and palaeoclimate evidence.

1. Introduction

There is currently significant uncertainty in the sensitivity of Earth's climate to radiative forcing, with the IPCC Assessment Report 5 (IPCC, 2013) estimating that the Equilibrium Climate Sensitivity (ECS, measuring the surface temperature response in °C to a sustained doubling of CO_2) ranges from 1.5 °C to 4.5 °C (Fig. 1a, black). This 1.5 to 4.5 °C range from IPCC (2013) incorporates many separate estimates of the ECS that have been made from multiple lines of evidence (e.g. see Knutti et al., 2017 see Figure 2 therein). Now consider a small selection of estimates chosen to reflect evidence from current energy budgets, complex Earth system models, and modern and geological observations. Estimates from energy balance considerations of the current transient climate system (Otto et al., 2013; Lewis and Curry et al., 2014) imply a best estimate ECS towards the lower end of the IPCC range (Fig. 1a, dark gray) of circa 1.6 to 2 °C. In contrast, analysis of the century timescale ECS from observation-constrained climate models (Cox et al., 2018), or from a combination of observational and geological constraints (Goodwin et al., 2018), suggests best estimate values from the middle of the IPCC range (Fig. 1a, light grey) of circa 3 °C. Together with this uncertainty in the value of the ECS is a growing acknowledgement that the Earth's climate sensitivity is likely to evolve through time, both due to time-evolving processes included within climate models (Armour et al., 2013; Knutti and Rugenstein, 2017; Williams et al., 2008; Andrews et al., 2015; Caldwell et al., 2016; Figure 2a), and over longer geological timescales (Zeebe, 2013; Rohling et al, 2018).

In a simple 1-dimensional energy balance model, the global mean surface warming at time t, $\Delta T(t)$ in °C, is empirically linked to the difference between total radiative forcing, $R_{total}(t)$ in Wm^{-2}, and the Earth's net energy imbalance, $N(t)$ in Wm^{-2}, via an effective climate feedback parameter, λ in $Wm^{-2}K^{-1}$, via

$$\lambda \Delta T(t) = R_{total}(t) - N(t), \qquad (1)$$

where, the total radiative forcing is a sum from i independent sources, $R_{total}(t) = \sum_i R_i(t)$, and the effective climate feedback parameter is defined such that $\lambda\Delta T(t)$ represents the total

aggregated outgoing radiative response in Wm^{-2} to the surface warming accounting for all feedback processes. Note that the word 'effective' is used here to suggest that the value of the climate feedback may represent an aggregated response, composed of different climate feedback values relating to different sources of radiative forcing, that may be changing through time.

However, there are a number of important deficiencies in this approach, which have been illustrated by applying this equation to the output of complex climate models. Firstly, the effective climate feedback parameter, λ, is not expected to remain constant in time, but instead display transient behaviour as different climate feedbacks respond to the imposed forcing over different timescales (e.g. Andrews and Webb, 2018; Caldwell et al. 2016; Knutti & Rugenstein, 2017; Zeebe, 2013; PALAEOSENS, 2012; Rohling et al., 2018; Senior and Mitchell, 2000; Gregory et al., 2004; Williams et al., 2008; Armour et al., 2013; Paynter et al., 2018; see Figure 2a). Secondly, λ may be different for different sources of radiative forcing, potentially arising due to the different spatial patterns of radiative forcing from different agents (Hansen et al. 2005; Marvel et al., 2016; Gregory and Andrews, 2016). Thirdly, in some models the ocean heat uptake (the dominant component of N), can have a larger effect on warming during transient climate change than an equivalent magnitude of radiative forcing, R, (e.g. Winton et al., 2010; Geoffroy et al., 2013; Frölicher et al., 2014).

Potentially, the discrepancy between climate sensitivity estimates derived from the Earth's current transient state energy balance (Otto et al, 2013; Lewis and Curry, 2014) and climate sensitivity estimates for century timescales (Cox et al., 2018; Goodwin et al., 2018) may be linked to the deficiencies in equation (1) (Fig. 1, compare dark and light gray). For example, λ may change over time between the current transient state and century timescales, the spatial pattern of radiative forcing and relative contributions from each agent today may not apply in the future, and the large current value of N in the current transient state may reduce as the system approaches a new steady state.

Without explicitly putting a time-dependence on the climate feedback, the simple 1-dimensional energy balance model (1) has been extended (e.g. Hansen et al., 2005; Winton et al, 2010; Geoffroy et al., 2013; Frölicher et al., 2014; Marvel et al., 2016; Goodwin et al.,

2015) by considering non-dimensional efficacy weighting on both the contributions to radiative forcing, ε_i, and the Earth's energy imbalance, ε_N, via,

$$\lambda \Delta T(t) = R_{total}^{weighted}(t) - \varepsilon_N N(t) \,, \qquad (2)$$

where the total efficacy weighted radiative forcing at time t is the sum of contributions from i independently time-varying sources with each contribution weighted by a non-dimensional efficacy term ε_i, $R_{total}^{weighted}(t) = \sum_i \varepsilon_i R_i(t)$ (Marvel et al., 2015), and $\varepsilon_N N(t)$ in Wm^{-2} represents the total efficacy-weighted energy imbalance of the Earth system.

Goodwin et al. (2018) utilised this extended 1-dimensional energy balance model (2), with efficacy-weighting but with climate feedback assumed constant in time, to drive an efficient Earth system model, generating history-matched projections of future warming and constraining century-timescale climate sensitivity (Fig. 1a, light gray). Instead of applying efficacy weightings (2), this study explores an alternative approach: Here, the energy balance equation (1) is extended to explicitly include time-varying climate feedbacks from multiple processes, that each respond independently to multiple radiative forcing agents. This extended energy balance equation is then used to constrain the climate sensitivity over multiple timescales, and used to show that this may explain the discrepancy between climate sensitivity estimates from the current transient energy balance and century timescale approaches (Fig. 1).

Section 2 derives the extended 1-dimensional energy balance model with j climate feedbacks independently responding over time to i radiative forcing agents. Section 3 then describes how the Warming Acidification and Sea level Projector (WASP) model (Goodwin, 2016; Goodwin et al., 2018) is extended to incorporate this extended energy balance equation and used to perform a large ensemble of climate simulations, where the initial distributions for the climate feedback strengths for the j processes are taken from the range of feedback strengths in the CMIP5 model ensemble analysed by Caldwell et al. (2016) and Andrews et al. (2015). A history matching approach (Williamson et al., 2015) is then applied, after Goodwin et al. (2018), to extract combinations of feedback strengths that are consistent with observational constraints (Table 2) for surface warming (Morice et al., 2012; GISSTEMP, 2018; Hansen et

al, 2010; Smith et al., 2008; Vose et al., 2012), ocean heat uptake (Levitus et al., 2012; Giese et al., 2011; Balmeseda et al., 2013; Good et al., 2013; Smith et al., 2015; Cheng et al., 2017; Kennedy et al., 2011; Huang et al., 2015) and carbon fluxes (IPCC, 2013 for 90% confidence bounds, based on original data now summarized in Le Quéré et al., 2018). Section 4 presents the history-matched results, evaluating the timescale evolutions of climate feedback, climate sensitivity and future warming that are consistent with observational and CMIP5 constraints. Section 5 discusses the wider implications of this study.

2. Time-evolving climate feedbacks

Consider a climate system where there are i independently time-varying sources of radiative forcing, $R_i(t)$ in Wm^{-2}, such that the total radiative forcing is written,

$$R_{total}(t) = \sum_i R_i(t). \quad (3)$$

The i different sources of radiative forcing include radiative forcing from atmospheric CO_2, other well-mixed greenhouse gases such as methane and nitrous oxide, solar forcing, and spatially localised forcing such as tropospheric aerosols and volcanic stratospheric aerosols (Figure 3).

In response to each of the i source of radiative forcing there are j independently time-evolving climate feedback processes, $\lambda_{i,j}(t)$ in $Wm^{-2}\,K^{-1}$, such that the total climate feedback due to radiative forcing agent i is written

$$\lambda_i(t) = \lambda_{Planck} + \sum_j \lambda_{i,j}(t), \quad (4)$$

where λ_{Planck} is the Planck sensitivity, equal to around 3.15 $Wm^{-2}\,K^{-1}$ (Caldwell et al., 2016) and $\lambda_{i,j}(t)$ is the climate feedback from process j in response to forcing agent i. The j climate feedback processes include the combined water vapour – lapse rate feedback, fast cloud feedbacks, snow and sea-ice albedo feedbacks, and the slow cloud feedback occurring as the spatial pattern of SSTs change in response to warming over many decades (Figure 2a). These feedbacks from the j processes operate over a range of different timescales. For example, it

takes order 10 days for water vapour to respond to surface warming, but due to the presence of multi-year sea ice it may take years for the snow + sea-ice albedo to respond to an imposed forcing, while it may take many decades for SST warming patterns to adjust towards an equilibrium state, thereby altering cloud feedback (Andrews et al., 2015).

The aim is to derive a modified energy balance equation that solves for the global mean surface temperature anomaly over time, $\Delta T(t)$, explicitly accounting for the independence of the *j* climate feedback responses to each of the *i* sources of radiative forcing. First, the general 1-D energy balance equation, (1), is re-arranged to solve for warming in terms of the ratio of the total radiative forcing $R_{total}(t)$ (Figure 3b) to the overall effective climate feedback $\lambda(t)$,

$$\Delta T(t) = \left(1 - \frac{N(t)}{R_{total}(t)}\right)\left(\frac{R_{total}(t)}{\lambda(t)}\right). \quad (5)$$

Next, we notice from (5) that the total radiative forcing divided by the overall effective climate feedback parameter at time *t*, $R_{total}(t)/\lambda(t)$, represents the overall warming that would be achieved from all sources of radiative forcing if the global climate system were in energy balance, $N(t) = 0$, via

$$\Delta T\big|_{N(t)=0}(t) = \left(\frac{R_{total}(t)}{\lambda(t)}\right). \quad (6)$$

We now state, by definition, that the radiative forcing from the *i*th agent divided by the climate feedback parameter for the *i*th agent at time *t*, $R_i(t)/\lambda_i(t)$, similarly represents the warming that would be achieved from radiative forcing by the *i*th agent if the global energy system were brought into balance, $N(t) = 0$, via

$$\Delta T_i\big|_{N(t)=0}(t) = \left(\frac{R_i(t)}{\lambda_i(t)}\right). \quad (7)$$

Now, it is assumed that the radiative forcing from all *i* sources is separable. This is reasonable if either the *i* sources of radiative forcing affect the absorption of different radiation

wavelengths, or the absorption of radiation at a given wavelength by one agent is independent of the absorption at the same wavelength by another. Note that while the radiative forcing from CH_4 and N_2O do have a dependence upon one another (Myhre et al, 2013), for the WASP experiments here these terms are combined into a single source of radiative forcing representing all greenhouse gases other than CO_2 (Figure 3, blue), which can be considered separable from the other agents.

Under the separable radiative forcing assumption for the *i* agents, the total warming from all sources of radiative forcing if the system is brought into energy balance must be equal to the sum of warming contributions from all *i* sources of radiative forcing at energy balance, $\sum_i \Delta T_i\big|_{N(t)=0}(t) = \Delta T\big|_{N(t)=0}(t)$. This allows us to write from (6) and (7),

$$\sum_i \left[\frac{R_i(t)}{\lambda_i(t)}\right] = \frac{R_{total}(t)}{\lambda(t)}. \qquad (8)$$

Substituting (8) into (5) gives an expression for global mean surface warming at time *t* as a function of the separate radiative forcing and climate feedback parameters for the *i* forcing agents,

$$\Delta T(t) = \left(1 - \frac{N(t)}{R_{total}(t)}\right)\sum_i \left[\frac{R_i(t)}{\lambda_i(t)}\right], \qquad (9)$$

The total modified energy balance equation for global mean surface warming from *j* climate feedback processes, which each evolve independently in response to *i* radiative forcing agents, is found by substituting (4) into (9) to reveal,

$$\Delta T(t) = \left(1 - \frac{N(t)}{R_{total}(t)}\right)\sum_i \left[\frac{R_i(t)}{\lambda_{Planck} + \sum_j \lambda_{i,j}(t)}\right]. \qquad (10)$$

Note that the total warming from the i different forcing agents when $N \neq 0$ is not equal to the sum of warming if each of the i agents acted alone in this energy balance equation, (10). This is because the ratio $N(t)/R_{total}(t)$ in equation (10) evolves according to the combined history of radiative forcing from all forcing agents, and would be different for the individual forcing agents acting alone (Figure 3).

The next section applies this energy balance equation (10), with independently time-varying forcing and feedbacks, to drive the efficient WASP Earth system model (Goodwin, 2016; Goodwin et al., 2018).

3. Numerical Earth system model with modified energy balance equation

WASP (Goodwin, 2016; Goodwin et al., 2018) is an efficient Earth system model that solves for global mean surface warming for carbon emissions scenarios using an energy balance equation with coupled carbon cycle terms (Goodwin et al., 2015). The WASP configuration of Goodwin et al. (2018) assumed a constant value for the effective climate feedback over time, λ, and applied non-dimensional efficacy weightings to heat uptake, N, and to the radiative forcing from aerosols, $R_{aerosol}$, equation (2). Here, we modify the WASP model by solving for global mean surface warming using equation (10), allowing climate feedback to vary over time independently for each forcing agent, and removing the non-dimensional efficacy weightings for heat imbalance and the different sources of radiative forcing.

3.1 Time dependent climate feedbacks in WASP

This section, and Appendix A, present the alterations made to the WASP model configuration of Goodwin et al. (2018) to enable warming to be calculated via equation (10). The full code for this version of the WASP model is available in Supplementary Information.

Consider a step function in the radiative forcing from agent i at time $t=t_0$, $R_i(t \geq t_0) \neq 0$, where $R_i(t<t_0)=0$. Initially, at time $t=t_0$ the climate feedback to agent i is given by the Planck feedback, $\lambda_i(t=t_0) = \lambda_{Planck}$. Here, we assume that the climate feedback contributions from the j climate processes then evolve towards their equilibrium values, $\lambda_{i,j}^{equil}$, with e-folding timescales for each process, τ_j. Thus, the overall climate feedback parameter, following a step-function for the ith source of radiative forcing, from all j processes at time $t_0+\Delta t$, $\lambda_i(t_0+\Delta t)$, becomes,

$$I_i(t_0 + \Delta t) = \sum_j I_{i,j}^{equil}\left(1 - \exp\left(\frac{-\Delta t}{t_j}\right)\right). \quad (11)$$

In the general case radiative forcing from each agent does not increase via a step function, but instead by pathways that can increase or decrease over time (Figure 3a). This is achieved in WASP by using two time-stepping equations (see Appendix): one equation adjusting the climate feedbacks to the existing radiative forcing to the *i*th source at the previous time-step, and a second equation adjusting the climate feedback to the additional radiative forcing from the *i*th source since the previous time-step, to account for the feedback to any additional radiative forcing being the Planck feedback initially. Full details are given in the Appendix.

Other alterations to the WASP model, from the configuration of Goodwin et al. (2018), include:
(1) the time-step is reduced from 1/12th of a year to 1/48th of a year (Appendix A), and
(2) the equations calculating the heat imbalance, *N* (see Goodwin, 2016; equations 3 and 4 therein), are altered to reflect the multiple time-varying climate feedback terms in (10) (Appendix A).

Separate radiative forcing terms from CO_2, other Well Mixed Greenhouse Gasses (WMGHG) and tropospheric aerosols are retained from the configuration of Goodwin et al. (2018) (Figure 3a), after Meinshausen et al. (2011), while solar radiative forcing (Meinshausen et al. 2011) and volcanic radiative forcing (from NASA GISS record, https://data.giss.nasa.gov/modelforce/strataer/; see Bouassa et al., 2012) are added (Figure 3a). The volcanic radiative forcing is added using the NASA record of Aerosol Optical Depth (AOD) since 1850 and applying a multiplier of -19±0.5 Wm^{-2} per unit AOD (Gregory et al., 2016), where the uncertainty represents the standard deviation of the multiplier between the different models in the ensemble. Where the time-resolution of radiative forcing (or atmospheric composition) is less than 1/48th of a year, the values are linearly interpolated between time-steps.

3.2 Generating an ensemble constrained by observations and CMIP5

This section details the construction of the very large initial Monte Carlo model ensemble, and the subsequent history matching used to extract the smaller final ensemble of constrained

model simulations. First, an initial ensemble of 10^7 simulations is generated with the strength of climate feedback from different processes taken from analysis of CMIP5 models by Caldwell et al. (2016) and Andrews et al. (2015) (Table 1; Figure 2a). All other model parameters are varied with input distributions after the configuration of Goodwin et al. (2018 – see Supplementary Table 2 therein).

The random-normal input distributions of climate feedback at equilibrium from Planck feedback, λ_{Planck}, combined Water Vapour Lapse Rate (WVLR), λ_{WVLR}, fast cloud adjustment, $\lambda_{FastCloud}$ and albedo adjustment, λ_{albedo}, (Table 1) are taken from analysis of these feedbacks in CMIP5 models by Caldwell et al (2016). The random-normal input distribution of climate feedback at equilibrium from the SST warming pattern adjustment-cloud feedback, $\lambda_{SlowCloud}$, is taken from the change in cloud feedback over time in CMIP5 models analysed by Andrews et al. (2015). These feedbacks are imposed with different input distributions for the timescales, τ_j (Table 1), with λ_{Planck} assumed to act instantaneously in all model simulations (Table 1).

The timescales for water-vapour lapse rate, τ_{WVLR}, and fast cloud feedback, $\tau_{\mathrm{FastCloud}}$, are varied with random-normal input distributions set to the residence time of water vapour in the atmosphere of 8.8±0.4 days (Ent and Tuinenburg, 2017). The global surface albedo feedback is found by Colman (2013) to have components acting from seasonal up to decadal timescales, presumably reflecting fast snow responses up to slower multi-year sea-ice responses. To simulate this range, the timescale for the snow and sea-ice albedo feedback, τ_{albedo}, is varied with a random distribution between 0.5 and 5 years (Table 1). The timescale for the slow cloud-SST adjustment feedback, $\tau_{SlowCloud}$, is varied with a random distribution from 20 to 45 years. The lower limit of 20 years is set by the initial time window Andrews et al. (2015) used to assess the response of CMIP5 models before the $\lambda_{SlowCloud}$ feedback applied. The upper limit of 45 years is (1) set to ensure that there are enough e-folding timescales for the $\lambda_{SlowCloud}$ feedback to take effect in the CMIP5 model simulations analysed by Andrews et al. (2015), and (2) set equal to a timescale for the thermocline identified by Fine et al. (2017), since spatial adjustment of SST warming patterns is likely linked to adjustments within the thermocline.

The combination of input distributions for feedback strengths, $\lambda_{i,j}$, and timescales, τ_j, (Table 1) results in a wide range of climate feedback over time in the initial 10^7-simulation ensemble (Figure 2b, gray).

The same values of climate feedback at equilibrium from each process are applied here to each source of radiative forcing (Table 1), except that the snow and sea-ice albedo feedback is reduced to 20% for volcanic stratospheric aerosol forcing compared to the other sources of radiative forcing (Table 1). This reflects the finding by Gregory et al. (2016) that in a CMIP5 model volcanic aerosols cause around 1.4 times less warming or cooling than an equivalent radiative forcing from CO_2. Here, this is imposed in the model by reducing the snow and sea ice albedo feedback term for volcanic aerosols, because the majority of volcanic forcing occurs at low latitudes and the majority of snow and sea-ice albedo forcing occurs at high latitudes. Note that in general the method applied here allows the strength of each climate feedback at equilibrium, $\lambda_{i,j}^{equil}$, to be independently assigned for each source of radiative forcing, (4) and (10), to reflect the different sensitivity of warming to each source of radiative forcing (e.g. Hansen et al., 2005; Marvel et al., 2016). However, a full exploration of this within the WASP model is reserved for future study.

Following the methodology of Goodwin et al. (2018), each of the 10^7 initial Monte Carlo prior simulations is then integrated to year 2017 and tested against observational metrics of surface warming, ocean heat uptake and ocean carbon uptake (Table 2). From the initial 10^7 simulations, 4.6×10^3 simulations agree with the observational constraints (Table 2) and are extracted to form a final posterior history matched (Williamson et al., 2015) ensemble (Figure 4a).

This final history matched ensemble of 4.6×10^3 simulations has climate feedback strengths consistent with the CMIP5 ensemble for multiple processes (Table 1), but shows simulated warming more tightly constrained by historical observations (Table 2) than for the range 13 CMIP5 models (Figure 4a, compare blue and beige to black; Appendix).

The observational constraints for surface warming compare time-average global temperature anomalies spanning ten-years or longer (Table 2). Therefore, the observed temperature anomaly response to volcanic forcing from months to a few years (e.g. Figure 4b, black) has

not been used to select the final history matched WASP model simulations. The simulated response of the history-matched WASP model ensemble to a recent volcanic eruption shows good agreement to the observed response for the real climate system (Figure 4b, compare black to blue), both in terms of the magnitude of cooling and the relative timing from the AOD perturbation. Although the ensemble simulated cooling is slightly larger than the observed cooling (Figure 4b), it should be noted that real system includes both the cooling effect of the volcanic eruption and the warming effect of the 1991/1992 El Nino event (Lehner et al., 2016). Accounting for this El Nino event may further improve the model-observation agreement. It should also be noted that the simulations record significantly greater cooling following the Krakatoa eruption in the late 19th century than is observed (Figure 4a). This is likely due to complexity in the climate system not included within the WASP model, with observations reflecting both the simultaneous actions of both volcanic activity and natural variability, and the complex regional patterns of temperature anomaly. For example, observations reflect that the 0 to 30°S and 0 to 30°N latitudinal regions both saw cooling in the months following the Krakatoa eruption, but the 30 °N to 90 °N region saw a warming (Robock and Mau, 1995 - Figure 4 therein). The agreement with observations of monthly to sub-decadal timescale cooling from a recent volcanic eruption (Figure 4b), being over a different timescale than the observational constraints (Table 2), provides an independent test showing that the time-varying climate feedback approach (10) is functioning appropriately in the WASP model.

4. Results

This section presents the results for the constrained distributions of climate feedback and climate sensitivity over different response timescales, and future warming projections, from the history matched WASP ensemble.

4.1 Constraints on climate feedback and climate sensitivity over time

The climate feedback to an imposed radiative forcing alters with the response timescale, depending on the processes that act over the different timescales (Figure 2a). In the experiments carried out here, a wide range of initial climate feedback strengths for different processes are used (Figure 2b, gray; Table 1), based on analysis of climate feedback in the CMIP5 models (Caldwell et al, 2016; Andrews et al., 2015).

Observational constraints are then applied to extract the posterior history matched WASP ensemble (Table 2), and the range of climate feedback over different response timescales narrows (Figure 2b, compare blue to gray; Table 1). Starting at the Planck feedback on very short timescales, the constrained estimate of climate feedback quickly decreases to 1.9±0.3 $Wm^{-2}\,K^{-1}$ on a response timescale of 0.1 years (Figure 2b, blue), and then slowly decreases further to around 1.5±0.3 $Wm^{-2}\,K^{-1}$ and 1.3±0.3 $Wm^{-2}\,K^{-1}$ on response timescales of 10 years and 100 years respectively.

The climate sensitivity (in °C) is defined as the radiative forcing for a doubling of CO_2 (in Wm^{-2}) divided by the climate feedback (in $Wm^{-2}\,K^{-1}$). Here, this definition is used to convert the constrained estimate of the climate feedback (Figure 2b, blue) into a constrained estimate for the evolution of the climate sensitivity over multiple response timescales (Figure 1; Table 3). The mean constrained estimate of climate sensitivity increases quickly to around 2 °C (ranging from 1.5 to 2.8 °C at 95%) on response timescales of 0.1 to 1 year (Figure 1, Table 3), before slowly increasing further to 2.9 °C (ranging from 1.9 to 4.6 °C at 95 %) over a response timescale of 100 years.

The 1-year response timescale climate sensitivity identified here is in good agreement with previous estimates from Earth's current transient energy balance, in which the anthropogenic radiative forcing is increasing annually (Figure 1, compare red to dark gray; Lewis and Curry, 2014; Otto et al., 2013). The 100-year response timescale climate sensitivity identified here is in good agreement with previous estimates for the equilibrium sensitivity, either using an emergent constraint on CMIP5 models or from combining palaeo-climate and historical observations (Figure 1, compare blue to light gray; Cox et al., 2018; Goodwin et al., 2018).

4.2 Constraints on the future warming response

The warming projections from the WASP ensemble (Figure 5, blue) are similar to the projections from a range of 13 CMIP5 models (Figure 5, beige; Appendix) for both RCP8.5 and RCP4.5 scenarios (Meinshausen et al., 2011). This broad agreement from differing approaches, one using complex models and another using a more efficient model with history matching, provides additional confidence in the future projections (Figure 5, blue and beige). The WASP projections do show narrower uncertainty range in future warming than the CMIP5 models. Possible reasons for this narrowing of future warming in WASP include the greater inter-annual and inter-decadal variability inherent in the CMIP5 models, and the

narrower ranges in simulated warming and ocean heat uptake imposed for the present day in WASP, due to the tighter observational constraints placed for historic warming and ocean heat uptake (Table 2; Figure 4). The RCP4.5 scenario does have a reduced chance of remaining under 2 °C warming for the 21st century (less than 1% likelihood) in the observationally constrained WASP projections, compared to CMIP5 models (Figure 5b, compare blue and beige). This is in agreement with the observationally constrained future warming projections of Goodwin et al. (2018) using a version of the WASP model in which the climate feedback is assumed constant in time.

5. Discussion

A modified energy balance equation is presented in which there is no single climate feedback applicable to all sources of radiative forcing at time *t*, $\lambda(t)$. Instead, surface warming is calculated using separate the climate feedbacks for each of the *i* sources of radiative forcing at time *t*, $\lambda_i(t)$, that are independently calculated from a set of *j* feedback-processes, $\lambda_{i,j}(t)$, via

$$\Delta T(t) = \left(1 - \frac{N(t)}{R_{total}(t)}\right) \sum_i \left[\frac{R_i(t)}{\lambda_{Planck} + \sum_j \lambda_{i,j}(t)} \right]. \quad (10)$$

Using the ranges of climate feedbacks for different processes analysed for CMIP5 models as a starting point (Table 1; see Caldwell et al. 2016; Andrews et al. 2015), a large ensemble of climate simulations driven by (10) are constructed, and then observational constraints are applied to extract a final history matched ensemble after Goodwin et al. (2018): (Table 2; Figure 4).

The final posterior history matched ensemble constrains the climate feedback over multiple timescales (Figure 2b) consistent both with climate feedbacks displayed by the CMIP5 models (Table 1) and with observational constraints of historic warming, heat uptake and carbon uptake (Table 2, Figure 4).

Much previous research has gone into constraining the Equilibrium Climate Sensitivity (ECS, in °C), representing the temperature change at equilibrium following a sustained doubling of CO_2 (e.g. IPCC, 2013; Knutti and Rugenstein, 2017). However, in the viewpoint presented

here, equation (10), there is no ECS. Instead, the ECS is replaced by a time-evolving climate sensitivity that varies depending on the response timescale (Figure 1; Table 3). The analysis presented here constrains this time-evolving climate sensitivity from sub-annual response timescales up to 10^2 year timescales (Figure 2). However there are additional processes that will alter the climate feedback and climate sensitivity further on longer timescales (e.g. PALAEOSENS, 2012; Rohling et al. 2018; Zeebe, 2013), for example there is an ice-sheet albedo feedback potentially lasting tens of thousands of years. Therefore, the constraint on climate sensitivity for a 10^2 year response timescale presented here (Figure 1, Table 3) should not be considered a final 'equilibrium' climate sensitivity, but part of an on-going evolution of climate sensitivity over multiple response timescales (Knutti and Rugenstein, 2017).

Consider the seeming inconsistency between previous best-estimates of climate sensitivity (Figure 1), with Earth's current transient energy balance suggesting a best estimate of around 1.6 to 2 °C (Lewis and Curry, 2014; Otto et al., 2013) and century timescale analysis suggesting best-estimates of around 3 °C (Cox et al., 2018; Goodwin et al., 2018). The combined constraints from the CMIP5 ensemble (Table 1) and observations (Table 3) placed here on the climate sensitivity over response timescales from 0.1, 1 and 10 years (Table 3; Figure 1) are similar to previous estimates of the ECS evaluated from radiative forcing and energy budget constraints (Otto et al, 2013; Lewis & Curry 2014). This similarity is interpreted here as reflecting the short response timescales that the current energy balance of the Earth system has to respond to anthropogenic forcing. Thus, the results for the climate sensitivity over shorter response timescales presented here are consistent with these previous findings (Otto et al. 2013; Lewis and Curry, 2014).

The constraint placed here on the climate sensitivity on a response timescale of 100 years (Table 3; Figure 1) agrees very well with two recent estimates of the ECS considering century timescales; one based on the century-timescale response of CMIP5 models with similar autocorrelation lag-1 temperature anomaly properties to the observed climate system (Cox et al., 2018), and another based on a similar history matched approach as used here, but with climate feedback assumed constant over time and an initial prior distribution based on paleoclimate evidence rather than the CMIP5 models (Goodwin et al., 2018).

Thus, this study suggests an interpretation whereby these different previous estimates of climate sensitivity are not inconsistent, but merely reflect different response timescales of the

system (Figure 1). When planning emission pathways to avoid dangerous climate change over the entire 21st century, it is appropriate to consider a century response timescale for climate sensitivity. For this purpose, a best estimate 100-year response timescale climate sensitivity of 2.9 °C, with a 66 % range from 2.3 to 3.6 °C, is found (Table 3; Figure 1).

This study has used prescriptive input distributions for climate feedback terms based on the CMIP5 models (Table 1), and then applied observational constraints (Table 2) to refine the distributions and constrain the response-timescale evolutions of climate feedback and climate sensitivity (Figures 1 and 2). To adapt the method applied here to use less prescriptive input distributions, such that the output would be independent of the CMIP5 models and based solely on observations, the following issues would need to be considered. Firstly, one would only be able to have a single feedback term for each order of magnitude in timescale. For example the λ_{WVLR} and $\lambda_{\mathrm{FastCloud}}$ feedbacks operate over the same order of magnitude timescale and so would need to be combined into a single feedback term. Secondly, one would require an observational constraint generated using (shorter timescale) monthly temperature anomaly data, where the current constraints on surface temperature use a minimum of a ten-year average (Table 2). Such an observational constraint based on monthly temperature anomaly data could possibly be achieved by considering the mean simulated-to-observed difference in the monthly response to a volcanic eruption over a decade (Figure 4b). However, these approaches are beyond the scope of this study and are reserved for future work.

Constraining the Earth's climate sensitivity, and understanding its possible response timescale evolution, is critical for reducing uncertainty in future warming projections (e.g. Knutti and Rugenstein, 2015). The history matching method with the WASP model applied in this study not only identifies a probability distribution for climate sensitivity over multiple response timescales (Fig. 1), but also then produces future warming projections using this time-evolving distribution (Fig. 5).

Appendix

Appendix A: Changes to the WASP model to allow time-evolving climate feedbacks

To allow time-dependent climate feedbacks in the WASP model, the following alterations are made from the configuration of Goodwin et al. (2018). First, the time-step in the WASP model, δt, is reduced from 1/12th of a year in the configuration of Goodwin et al. (2018) to 1/48th of a year here.

The following equation adjusts the climate feedback to the existing radiative forcing from *i*th sources from time t to time $t+\delta t$, considering the j processes evolve towards their equilibrium feedback values according to their equilibrium timescales, τ_j (Table 1),

$$\lambda_i(t+\delta t) = \lambda_{Planck} + \sum_j \left[\left(\lambda_{i,j}^{equil} - \lambda_{i,j}(t) \right) \left(1 - \exp\left(\frac{-\delta t}{\tau_j} \right) \right) \right]. \quad \text{(A1)}$$

Any additional radiative forcing at time $t+\delta t$ relative to t will only operate at the Planck sensitivity, the other feedback terms from the j processes will be zero in this initial time-step. This is expressed by reducing the time-dependent contributions to climate feedback according to the absolute ratio of previous to new radiative forcing,

$$\lambda_{i,j}(t+\delta t) = \lambda_{i,j}(t) \left| \frac{R_i(t)}{R_i(t+\delta t)} \right|, \quad \text{(A2)}$$

noting that (A2) is only applied when the radiative forcing is growing in magnitude, $|R_i(t+\delta t)| > |R_i(t)|$. Note, numerically the absolute value is needed in (A2) because of occasions where R_i changes sign (e.g. solar forcing) – you don't want to swap the sign of lambda for process j, but reduce it to zero.

To calculate the heat imbalance at time t in WASP, $N(t)$ in Wm^{-2}, the radiative forcing is modulated by the fractional distance from equilibrium of the anthropogenic heat of the surface mixed layer, $H_{mix}(t)$ in J, using (Goodwin, 2016),

$$N(t) = \left(\frac{H_{mix}^{equil}(t) - H_{mix}(t)}{H_{mix}^{equil}(t)} \right) \sum_i R_i(t), \qquad \text{(A3)}$$

where $H_{mix}^{equil}(t)$ is the eventual heat uptake at equilibrium for the surface mixed layer in J if the radiative forcing at time *t* is held constant into the future. Here, allow the climate feedback for each source of radiative forcing to evolve independently in time, the equation calculating $H_{mix}^{equil}(t)$ is modified from the previous form (Goodwin, 2016, equation 3 therein) by summing R_i/λ_i for each of the *i*-sources of radiative forcing,

$$H_{mix}^{equil}(t) = r_{SST:SAT} V_{mix} c_P \sum_i \frac{R_i(t)}{\lambda_{i,j}(t)}, \qquad \text{(A4)}$$

where $r_{SST:SAT}$ is the ratio of warming of sea surface temperature to surface air-temperatures at equilibrium, V_{mix} is the volume of the surface mixed layer and c_P is the specific heat capacity of seawater.

Appendix B: Calculating and plotting temperature anomaly.

For the figures displayed the annual mean temperature anomalies are calculated as follows: the GISTEMP record is shown relative to the 1880 to 1900 average, the HadCRUT4 and WASP simulations are shown relative to the 1850 to 1900 average and the CMIP5 simulations shown relative to the 1861 to 1900 average.

The simulated warming ranges of 13 CMIP5 simulations plotted in Figures 4 and 5 include the CanESM2 (Arora et al., 2011), CESM1-BGC (Moore et al., 2013), GFDL-ESM2G (Dunne et al., 2013), GFDL-ESM2M (Dunne et al., 2013), HadGEM2-CC (Martin et al., 2011), HadGEM2-ES (Jones et al., 2011), IPSL-CM5A-LR (Dufresne et al., 2013), IPSL-CM5A-MR (Dufresne et al., 2013), IPSL-CM5B-LR (Dufresne et al., 2013), MIROC-ESM-CHEM (Watanabe et al., 2011), MIROC-ESM (Watanabe et al., 2011), MPI-ESM-LR Ref. 50 (Giorgetta et al., 2013) and NorESM1-ME (Tjiputra et al., 2013) models. The shaded regions in Figures 4 and 5 represent the range of annual mean surface warming values from the 13 CMIP5 models, using a single realization of each CMIP5 model. The warming is calculated relative to the 1861-1900 average within each simulation.

Acknowledgements

This research was funded by UK NERC grant number NE/N009789/1 and combined UK NERC/UK Government Department of BEIS grant number NE/P01495X/1. Comments from two anonymous reviewers improved the quality of the manuscript.

Supplementary Information and data availability

Two supplementary Information files give the full code for the WASP model described in this study (Goodwin-ds01.cpp and Goodwin-ds02.cpp). These files are configured to repeat all experiments presented in this study, and represent the data for this study.

References:

Andrews, T and M.J. Webb (2018). The Dependence of Global Cloud and Lapse Rate Feedbacks on the Spatial Structure of Tropical Pacific Warming, *Journal of Climate* https://doi.org/10.1175/JCLI-D-17-0087.1

Andrews, T., J.M. Gregory and M.J. Webb (2015) The Dependence of Radiative Forcing and Feedback on Evolving Patterns of Surface Temperature Change in Climate Models, *Journal of Climate* 28, p1630-1648, https://doi.org/10.1175/JCLI-D-14-00545.1

Armour, K.C., C.M. Bitz and G.H. Roe (2013) Time-Varying Climate Sensitivity from Regional Feedbacks, *Journal of Climate* 26, p4518-4534, https://doi.org/10.1175/JCLI-D-12-00544.1

Arora, V. K. et al. (2011). Carbon emission limits required to satisfy future representative concentration pathways of greenhouse gases. *Geophys. Res. Lett.* 38, L046270.

Balmaseda, M. A., Mogensen, K. & Weaver, A. T. (2013). Evaluation of the ECMWF ocean reanalysis system ORAS4. *Q. J. Roy. Meteorol. Soc.* 139, 1132–1161.

Bourassa, A.E., A. Robock, W.J. Randel, T. Deshler, L.A. Reiger, N.D. Lloyd, E.J. Llewellyn & D.A. Degenstein (2012). Large volcanic aerosol load in the stratosphere linked to Asian monsoon transport. *Science* 337, 78-81, doi:10.1126/science.1219371.

Caldwell, P.M., M.D. Zelinka, K.E. Taylor, and K. Marvel (2016). Quantifying the Sources of Intermodel Spread in Equilibrium Climate Sensitivity, *Journal of Climate* 29, 513-524, DOI:10.1175/JCLI-D-15-0352.1.

Cheng, L. et al. (2017). Improved estimates of ocean heat content from 1960 to 2015. *Sci. Adv.* 3, e1601545.

Cox, P.M., C. Huntingford & M.S. Williamson (2018). Emergent constraint on equilibrium climate sensitivity from global temperature variability, *Nature* 553, 319–322, doi:10.1038/nature25450.

Dufresne, J. L. et al. (2013). Climate change projections using the IPSL-CM5 Earth system model: from CMIP3 to CMIP5. *Climate Dynamics* 40, 2123–2165.

Dunne, J. P. et al. (2013). GFDLs ESM2 global coupled climate carbon Earth system models. Part II: Carbon system formulation and baseline simulation characteristics. J. Clim. 26, 2247–2267.

Frölicher TL, M. Winton & J.L. Sarmiento (2014) Continued global warming after CO2 emissions stoppage. *Nature Climate Change* 4:40–44

Geoffroy O. et al. (2013) Transient climate response in a two-layer energy-balance model. Part II: representation of the efficacy of deep-ocean heat uptake and validation for CMIP5 AOGCMs. *J. Clim* 26:1859–1876

Giese, B. S. & S. Ray. (2011). El Niño variability in simple ocean data assimilation (SODA), 1871–2008. *J. Geophys. Res*. 116, C02024.

Giorgetta, M. A. et al. (2013). Climate and carbon cycle changes from 1850 to 2100 in MPI-ESM simulations for the Coupled Model Intercomparison Project phase 5: climate changes in MPI-ESM. *J. Adv. Model. Earth Syst.* 5, 572–597.

GISS Surface Temperature Analysis (GISTEMP) (NASA Goddard Institute for Space Studies, accessed 5th April 2018); https://data.giss.nasa.gov/gistemp/

Good, S. A., M.J. Martin, & N.A. Rayner (2013). EN4: quality controlled ocean temperature and salinity profiles and monthly objective analyses with uncertainty estimates. *J. Geophys. Res. Ocean*. 118, 6704–6716.

Goodwin. P., A. Katavouta, V.M. Roussenov, G.L. Foster, E.J. Rohling and R.G. Williams, (2018) Pathways to 1.5 and 2 °C warming based on observational and geological constraints, *Nature Geoscience* 11, 102-107, doi:10.1038/s41561-017-0054-8.

Goodwin, P. (2016) How historic simulation-observation discrepancy affects future warming projections in a very large model ensemble, *Climate Dynamics*, CLDY-D-15-00368R2, doi: 10.1007/s00382-015-2960-z.

Goodwin, P., R.G. Williams and A. Ridgwell (2015), Sensitivity of climate to cumulative carbon emissions due to compensation of ocean heat and carbon uptake, *Nature Geoscience* 8, p29-34. doi:10.1038/ngeo2304.

Gregory, J.M. and T. Andrews (2016), Variation in climate sensitivity and feedback parameters during the historical period, *Geophysical Research Letters*, Volume 43, Issue 8, pages 3911–3920.

Gregory, J.M., T. Andrews, P. Good, T. Mauritsen, & P.M. Forster (2016) Small global-mean cooling due to volcanic radiative forcing, *Climate Dynamics* 47, 3979–3991, DOI 10.1007/s00382-016-3055-1.

Gregory, J. M., W. J. Ingram, M. A. Palmer, G. S. Jones, P. A. Stott, R. B. Thorpe, J. A. Lowe, T. C. Johns, and K. D. Williams (2004), A new method for diagnosing radiative forcing and climate sensitivity, *Geophys. Res. Lett.*, 31, L03205, doi:10.1029/2003GL018747.

Hansen, J., M. Sato, R. Ruedy, L. Nazarenko, A. Lacis, G. A. Schmidt, G. Russell, et al. (2005) Efficacy of climate forcings, *J. Geophys. Res.*, 110, D18104, doi:10.1029/2005JD005776.

Hansen, J., S. Ruedy, M. Sato & K. Lo (2012). Global surface temperature change. *Rev. Geophys*. 48, RG4004.

Huang, B. et al. (2015) Extended Reconstructed Sea Surface Temperature Version 4 (ERSST.v4). Part I: Upgrades and intercomparisons. *J. Clim*. 28, 911–930.

IPCC (2013) *Climate Change 2013: The Physical Science Basis* (eds Stocker, T. F. et al.) (Cambridge Univ. Press, Cambridge, 2013).

Jones, C. D. et al. (2011). The HadGEM2-ES implementation of CMIP5 centennial simulations. *Geosci. Model. Dev*. 4, 543–570.

Kennedy, J. J., Rayner, N. A., Smith, R. O., Saunby, M. & Parker, D. E. (2011). Reassessing biases and other uncertainties in sea-surface temperature observations measured in situ since 1850. Part 2: Biases and homogenisation. *J. Geophys. Res*. 116, D14104.

Knutti, R. and M.A.A. Rugenstein (2015) Feedbacks, climate sensitivity and the limits of linear models. *Phil. Trans. R. Soc. A* **373**: 20150146. http://dx.doi.org/10.1098/rsta.2015.0146

Knutti, R., M.A.A. Rugenstein and G.C. Hergerl (2017) Beyond equilibrium climate sensitivity, *Nature Geoscience* 10, 727-736, DOI:10.1038/ngeo3017.

Lehner, F., A. P. Schurer, G. C. Hegerl, C. Deser, and T. L. Frölicher (2016), The importance of ENSO phase during volcanic eruptions for detection and attribution, *Geophys. Res. Lett.*, 43(6), doi:10.1002/2016GL067935.

Levitus, S. et al. (2012). World ocean heat content and thermosteric sea level change (0–2000 m), 1955–2010. *Geophys. Res. Lett*. 39, 10.

Lewis, N. & J.A. Curry (2014) The implications for climate sensitivity of AR5 forcing and heat uptake estimates, Climate Dynamics 45, 1009-1023.

Martin, G. M. et al. (2011). The HadGEM2 family of Met Office Unified Model climate configurations. *Geosci. Model. Dev*. 4, 723–757.

Meinshausen, M. et al. (2011). The RCP greenhouse gas concentrations and theirextensions from 1765 to 2300. *Climatic Change* 109, 213–241.

Moore, J., Lindsay, K., Doney, S., Long, M. & Misumi, K. (2013). Marine ecosystem dynamics and biogeochemical cycling in the Community Earth System Model [CESM1(BGC)]: comparison of the 1990s with the 2090s under the RCP4.5 and RCP8.5 scenarios. J. Clim. 26, 9291–9312.

Morice, C. P., Kennedy, J. J., Rayner, N. A. & Jones, P. D. (2012). Quantifying uncertainties in global and regional temperature change using an ensemble of observational estimates: the HadCRUT4 dataset. *J. Geophys. Res*. 117, D08101.

Myhre, G., et al. (2013) Anthropogenic and Natural Radiative Forcing Supplementary Material. In: *Climate Change 2013: The Physical Science Basis. Contribution of Working Group I to the Fifth Assessment Report of the Intergovernmental Panel on Climate Change* [Stocker, T.F., D. Qin, G.-K. Plattner, M. Tignor, S.K. Allen, J. Boschung, A. Nauels, Y. Xia, V. Bex and P.M. Midgley (eds.)].

Otto, A., F.E.L. Otto, O. Boucher, J. Church, G. Hegerl, P.M. Forster, N.P. Gillett, et al. (2013) Energy budget constraints on climate response, *Nature Geoscience* 6, 415-416.

PALAEOSENS (2012). Making sense of palaeoclimate sensitivity. *Nature* 491, 683–691.

Paynter, D., T.L. Frölicher, L.W. Horowitz, and L.G. Silvers (2018), Equilibrium Climate Sensitivity Obtained From Multimillennial Runs of Two GFDL Climate Models, *J. Geophys. Res. Atmos.*, 123(4), 1921-1941, doi:10.1002/2017JD027885.

Robock, A., & J. Mau (1995) The Volcanic Signal in Surface Temperature Observations, *Journal of Climate*, 8, 1086-1102.

Rohling, E.J., G. Marino, G.L. Foster, P.A. Goodwin, A.S. von der Heydt, P. Köhler (2018) Comparing Climate Sensitivity, Past and Present, *Annual Review of Marine Science*,

10, pp.261–288. http://www.annualreviews.org/doi/full/10.1146/annurev-marine-121916-063242

Senior, C., and J. F. Mitchell (2000), The time-dependence of climate sensitivity, *Geophys. Res. Lett*., 27(17), 2685-2688, doi:10.1029/2000GL011373.

Smith, T. M., R.W. Reynolds, T.C. Peterson & J. Lawrimore (2008). Improvements to NOAA's historical merged land–ocean surface temperature analysis (1880–2006). *Journal of Climate* 21, 2283–2296.

Smith, D. M. et al. (2015). Earth's energy imbalance since 1960 in observations and CMIP5 models. *Geophys. Res. Lett.* 42.4, 1205–1213.

Tjiputra, J. F. et al. (2013). Evaluation of the carbon cycle components in the Norwegian Earth System Model (NorESM). *Geosci. Model. Dev*. 6, 301–325.

Vose, R. S. et al. (2012). NOAA's merged land–ocean surface temperature analysis. *Bull. Am. Meteorol. Soc.* 93, 1677–1685.

Watanabe, S. et al. (2011). MIROC-ESM 2010: model description and basic results of CMIP5-20c3m experiments. *Geosci. Model. Dev.* 4, 845–872.

Williams, K. D., W. J. Ingram, and J. M. Gregory (2008), Time Variation of Effective Climate Sensitivity in GCMs, *J. Clim.*, 21(19), 5076-5090, doi:10.1175/2008JCLI2371.1.

Williamson, D., A.T. Blaker, C. Hampton, & J. Salter (2015). Identifying and removing structural biases in climate models with history matching. *Climate Dynamics* 45, 1299-1324. DOI:10.1007/s00382-014-2378-z.

Winton M, Takahashi K, Held I (2010) Importance of ocean heat uptake efficacy to transient climate change. *Journal of Climate* 23:2333–2344

Zeebe, R.E. Time-dependent climate sensitivity and the legacy of anthropogenic greenhouse gas emissions, *Proc. Natl. Acad. Sci*., vol. 110 no. 34, 13739–13744, doi: 10.1073/pnas.1222843110

Table 1: Time-evolving climate feedbacks in the WASP model. All input distributions are identical for the different sources of radiative forcing, expect that for volcanic radiative forcing the snow + sea-ice albedo feedback is reduced to 20% of the value for other sources.

[a] Input distribution taken from the CMIP5 models as analyzed by Caldwell et al. (2016).

[b] Input distribution taken from the CMIP5 models as analyzed by Andrews et al. (2015).

Feedback process	**Equilibrium feedback input distribution**	**e-folding adjustment timescale input distribution**	**Posterior climate feedback (mean and standard deviation)**
Planck Feedback[a], $\lambda_{\square\square\square\square\square\square}$	Random-normal: μ = 3.15 $Wm^{-2}K^{-1}$ σ = 0.04 $Wm^{-2}K^{-1}$	Instantaneous	μ = 3.15 $Wm^{-2}K^{-1}$ σ = 0.04 $Wm^{-2}K^{-1}$
Combined water vapour-lapse rate feedback[a], λ_{WVLR}	Random-normal: μ = -1.15 $Wm^{-2}K^{-1}$ σ = 0.09 $Wm^{-2}K^{-1}$	Random-normal: μ = 8.9 days σ = 0.4 days	μ = -1.13 $Wm^{-2}K^{-1}$ σ = 0.09 $Wm^{-2}K^{-1}$
Fast cloud feedback[a] (initial transient SST patterns), $\lambda_{\square\square\square\square Clouds}$	Random-normal: μ = -0.43 $Wm^{-2}K^{-1}$ σ = 0.33 $Wm^{-2}K^{-1}$	Random-normal: μ = 8.9 days σ = 0.4 days	μ = -0.11 $Wm^{-2}K^{-1}$ σ = 0.26 $Wm^{-2}K^{-1}$
Snow + sea-ice albedo climate feedback[a], λ_{albedo}	Random-normal: μ = -0.37 $Wm^{-2}K^{-1}$ σ = 0.10 $Wm^{-2}K^{-1}$	Random: Min. = 0.5 years, Max. = 5.0 years	μ = -0.34 $Wm^{-2}K^{-1}$ σ = 0.10 $Wm^{-2}K^{-1}$
Cloud – spatial SST adjustment feedback[b], $\lambda_{SlowCloud}$	Random-normal: μ = -0.47 $Wm^{-2}K^{-1}$ σ = 0.30 $Wm^{-2}K^{-1}$	Random: Min. = 20 years, Max. = 45 year.	μ = -0.27 $Wm^{-2}K^{-1}$ σ = 0.28 $Wm^{-2}K^{-1}$

Table 2: Observational constraints and posterior simulated ranges. All constraints represent 90 or 95 % uncertainty ranges in the observed quantities. See Goodwin et al. (2018) for details.

Observational constraint	Observation-consistent range	Comment/References	Posterior 95 % range
Global mean temperature anomaly, 1986-2005 relative to 1850-1900	0.55 to 0.67 °C	Constraint amended from 2003-2012 period in Goodwin et al. (2018) to 1986-2005 period here, so that the final time-average includes a significant volcanic eruption. Range based on 90% observational range from IPCC (2013).	0.55 to 0.67 °C
Global mean temperature anomaly, 2007-2016 relative to 1971-1980	0.56 to 0.69 °C	Constraints and ranges as used in Goodwin et al. (2018). Based on: (Morice et al. 2012; GISTEMP, 2018; Hansen et al., 2010; Smith et al., 2008; Vose et al., 2012)	0.57 to 0.69 °C
Global mean temperature anomaly, 2007-2016 relative to 1951-1960	0.54 to 0.78 °C		0.63 to 0.76 °C
Global mean sea-surface temperature anomaly, 2003-2012 relative to 1850-1900	0.56 to 0.68 °C	Constraint and range as used in Goodwin et al. (2018). Based on (Kennedy et al., 2011; Huang et al., 2015)	0.56 to 0.68 °C
Whole ocean heat content anomaly, 2010 relative to 1971	117 to 332 ZJ	Constraints and ranges as used in Goodwin et al. (2018). Based on (Levitus et al., 2012; Giese et al., 2011; Balmaseda et al., 2013; Good et al., 2013; Smith et al., 2018; Cheng et al., 2017)	152 to 337 ZJ
Upper 700m ocean heat content anomaly, 2010 relative to 1971	98 to 170 ZJ		103 to 171 ZJ
Terrestrial carbon uptake, 2011 relative to preindustrial	70 to 250 PgC	Constraint and range as used in Goodwin et al. (2018). Based on IPCC (2013)	95 to 253 PgC
Rate of terrestrial carbon uptake, 2000 to 2009	1.4 to 3.8 PgC yr^{-1}	Constraint and range as used in Goodwin et al. (2018). Based on IPCC (2013)	1.3 to 3.6 PgC yr^{-1}
Ocean carbon uptake, 2011 relative to preindustrial	125 to 185 PgC	Constraint and range as used in Goodwin et al. (2018). Based on IPCC (2013)	126 to 181 PgC

Table 3: Constrained climate sensitivity estimates for multiple response timescales.

Response timescale, τ	Median Climate Sensitivity	66% range in Climate Sensitivity	95 % range in Climate Sensitivity
0.1 years	1.9 °C	1.7 to 2.2 °C	1.5 to 2.6 °C
1 years	2.1 °C	1.8 to 2.4 °C	1.6 to 2.8 °C
10 years	2.4 °C	2.1 to 2.9 °C	1.8 to 3.4 °C
100 years	2.9 °C	2.3 to 3.5 °C	1.9 to 4.6 °C

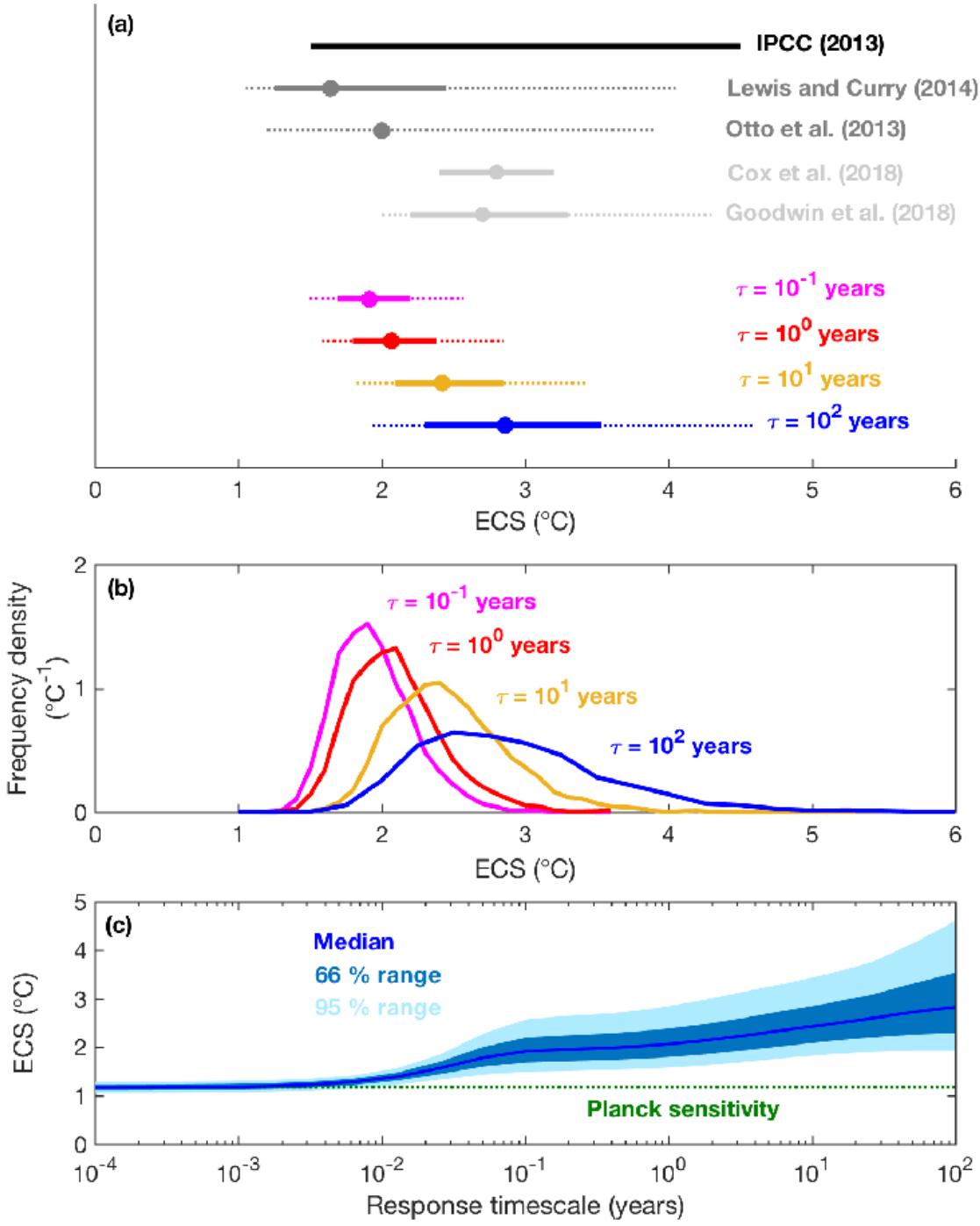

Figure 1: The constrained evolution of climate sensitivity over multiple response timescales. (a) Estimates of the climate sensitivity (°C) from multiple studies (black and gray) compared to the posterior history matched WASP ensembles in this study evaluated over multiple response timescales ranging from 10^{-1} to 10^{2} years (colors). Dots are best estimates (using median from distributions for this study), thick solid lines are 66 % ranges and dotted lines are 95 % ranges. (b) The frequency density distributions of climate sensitivity in the posterior history matched WASP ensembles over multiple response timescales. (c) The climate sensitivity (°C) over multiple response timescales in the posterior history matched WASP ensemble (blue, lines and shading show median and uncertainty ranges).

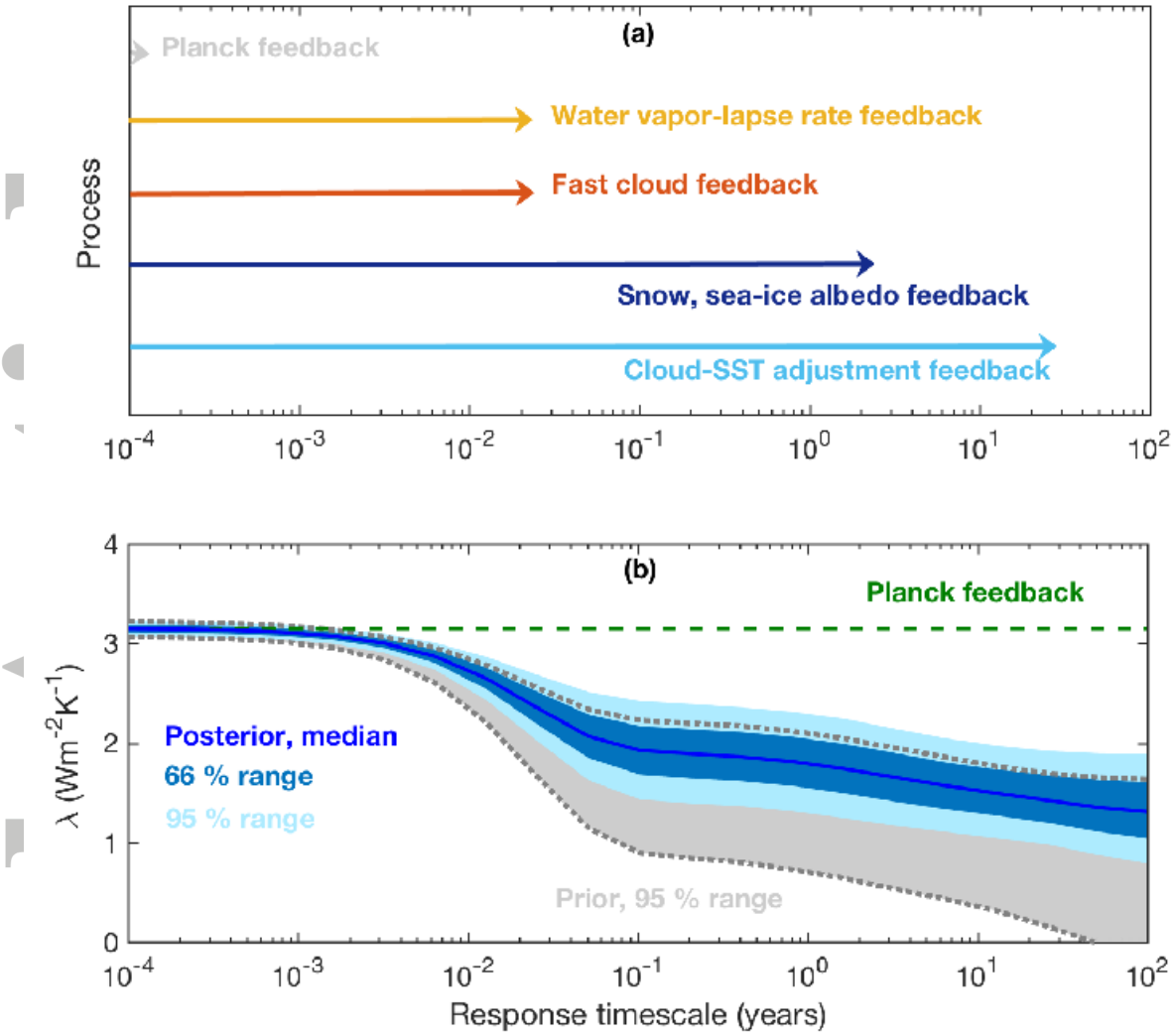

Figure 2: Time evolution of climate feedback over multiple timescales. (a) Schematic of different climate feedback processes considered in this study, and their characteristic response timescales. (b) The climate feedback over different response timescales in the initial prior model ensemble (grey: shaded area and dotted lines, showing 95% range) and in the final posterior history matched ensemble (blue, line is median, dark blue shading is 66% range, light blue shading is 95 % range). Also shown for comparison is the Planck sensitivity (green).

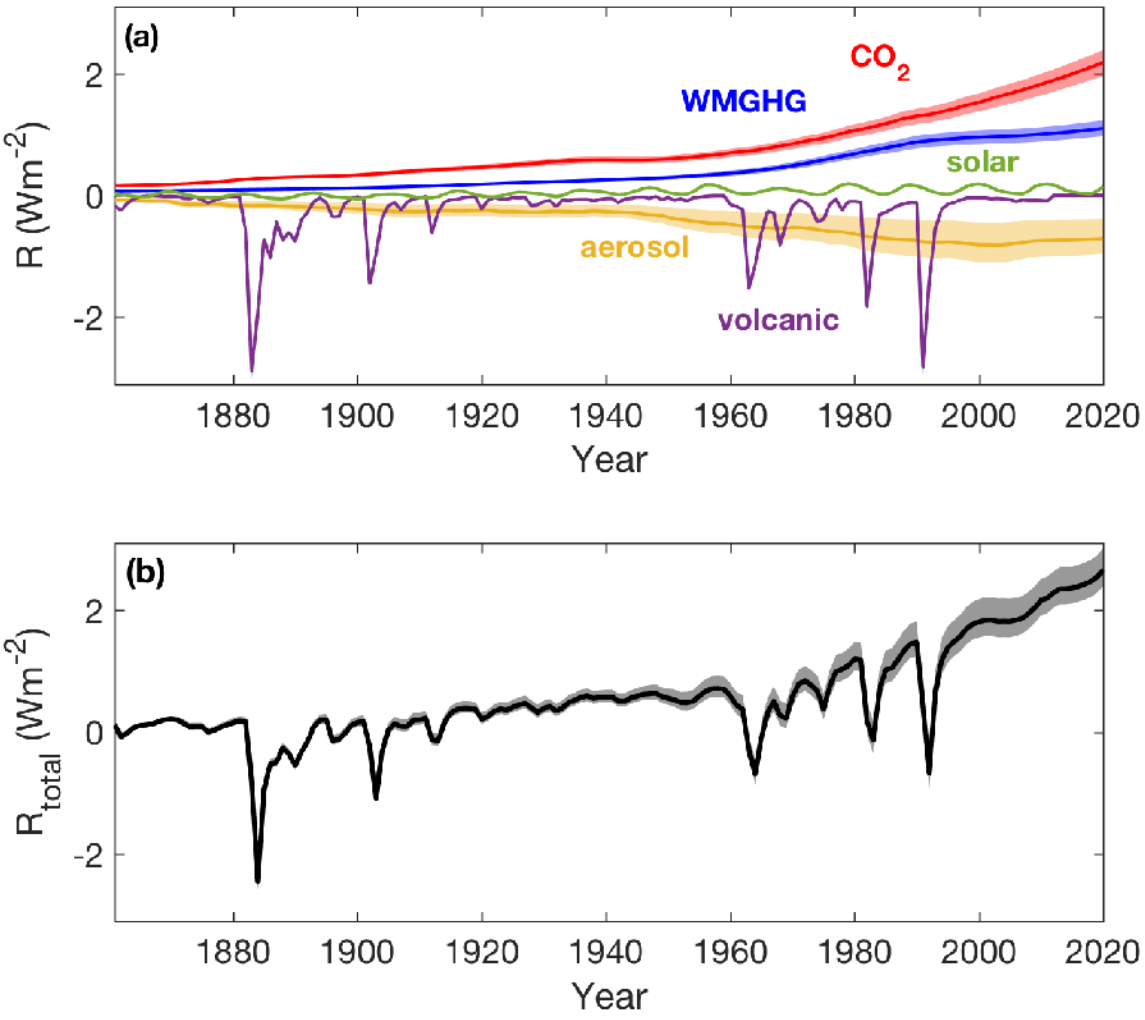

Figure 3. Applied radiative forcing over time. (a) Radiative forcing over time from multiple sources in the posterior history matched model ensemble, showing median (line) and 95% range (shading). The sources of radiative forcing are: atmospheric CO_2 (red), Well mixed Greenhouse Gasses (WMGHG) other than CO_2 (blue), tropospheric aerosols (orange), volcanic stratospheric aerosols (purple), and solar forcing (green). (b) The total radiative forcing from all sources, R_{total}, over time in the posterior history matched model ensemble (line is median, shaded area is 95% range). All radiative forcings are annually smoothed with the exception of volcanic aerosols, which have a monthly resolution.

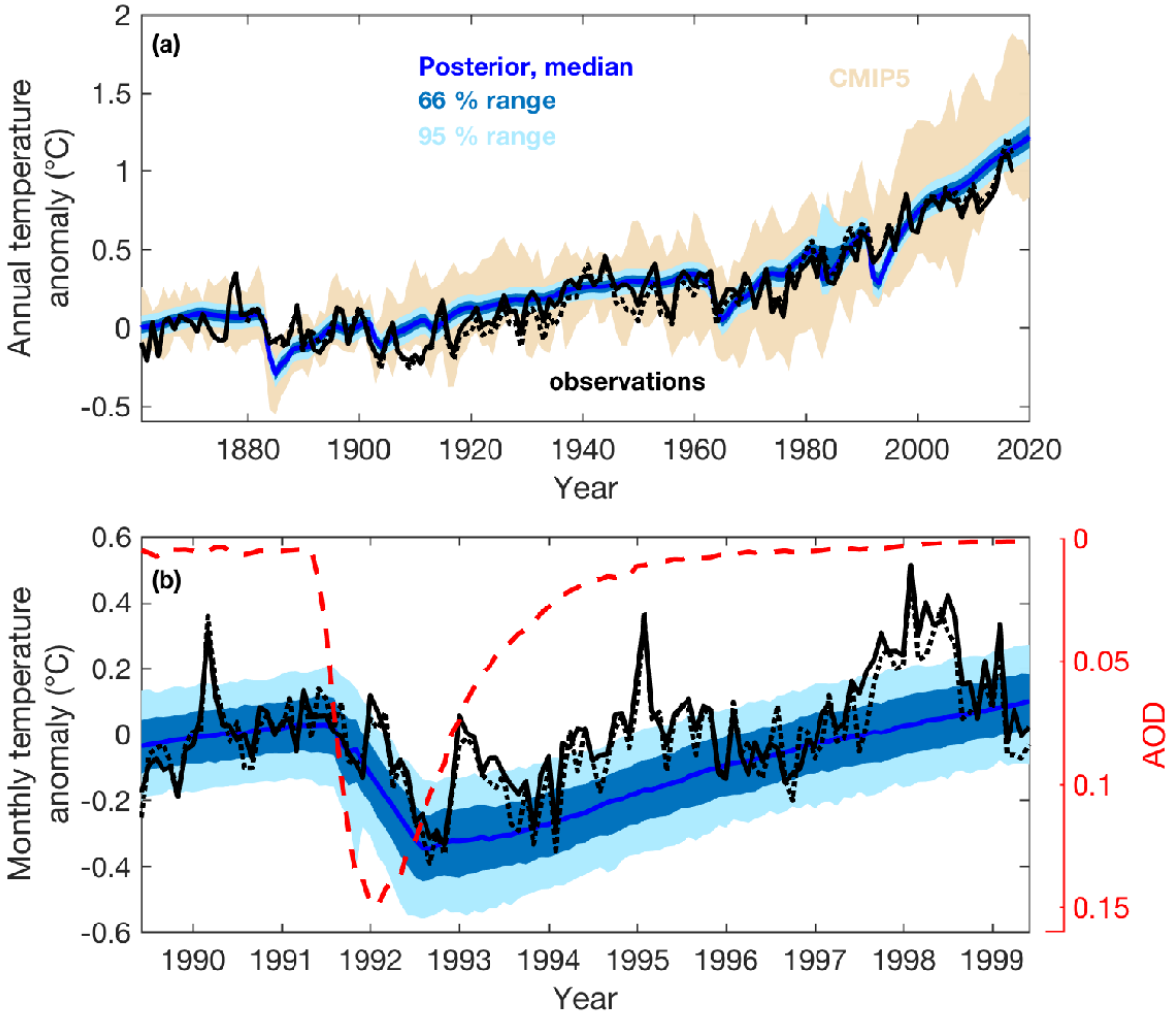

Figure 4. Observed and simulated temperature anomaly over time. (a) Annual mean temperature anomaly from 1861 to 2020. Shown are observations to (black: solid line is HadCRUT4 from 1861-2017, dotted line is GISTEMP from 1880 to 2017) and simulated temperature anomaly from the posterior WASP history matched ensemble of simulations with modified energy balance (blue, lines and shading as Figure 1b), and from 13 CMIP5 models (beige shading showing range). All annual temperature anomalies are shown relative to the pre-1900 average (Appendix B). (b) Monthly temperature anomaly before and after the eruption of Mt. Pinatubo from observations (black, as panel a) and the posterior history matched WASP ensemble simulations (blue, as panel a), and the AOD (red). Both observed and simulated monthly temperature anomalies are shown relative to the 2-year average prior to the eruption of Mt. Pinatubo.

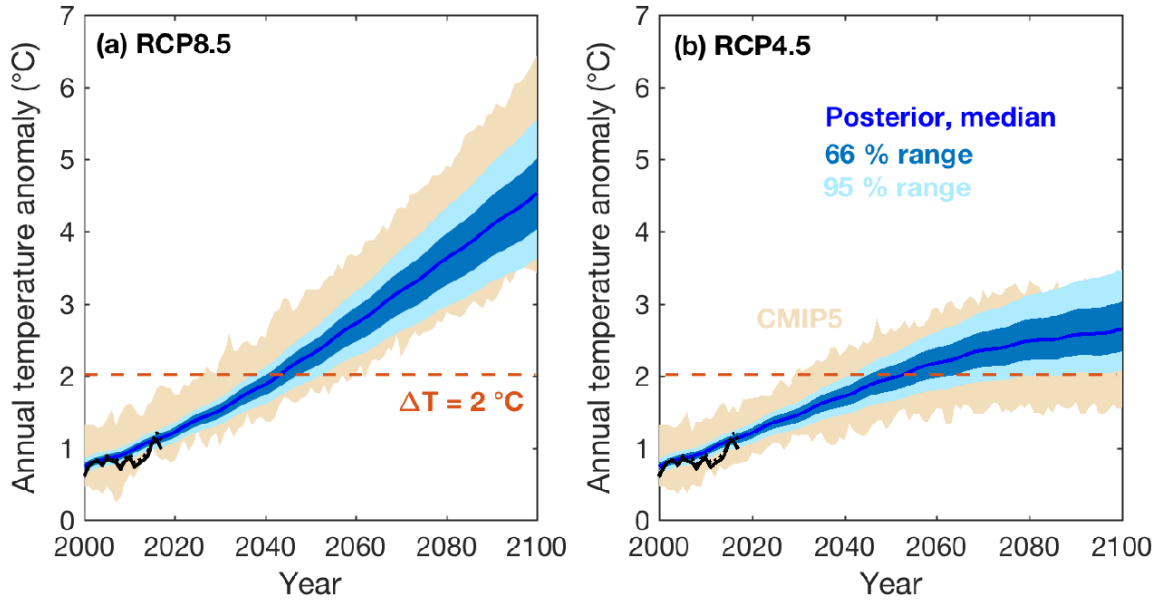

Figure 5: Warming over the 21st century. Future warming projections from the posterior history matched WASP ensemble (blue, line and shading as figure 1b) and a range of 13 CMIP5 Earth system models (beige shading showing range; see Appendix) for (a) RCP8.5 and (b) RCP4.5 scenarios. Also shown are observed warming from 2000 to 2017 (black lines: solid is HadCRUT4, dotted is GISTEMP).